New insights in the mechanism of the SARS-CoV-2 M^{pro} inhibition by benzisoselenazolones and diselenides

Luca Sancineto,[1] Francesca Mangiavacchi,[1] Agnieszka Dabrowska,[2,3] Agata J. Pacuła-Miszewska,[4] Magdalena Obieziurska-Fabisiak,[4] Cecilia Scimmi,[1] Veronica Ceccucci,[1] Juan Kong,[5] Yao Zhao,[5] Gianluca Ciancaleoni,[6] Vanessa Nascimento,[7] Bruno Rizzuti,[8,9] Anna Kula-Pacurar,[2] Haitao Yang,[5] Jacek Ścianowski,[4] Ying Lei,[5*] Krzysztof Pyrc[2*], and Claudio Santi.[1*]

1 Department of Pharmaceutical Sciences, University of Perugia, Via del Liceo 1, 06100 Perugia (PG), Italy
2 Virogenetics Laboratory of Virology, Malopolska Centre of Biotechnology, Jagiellonian University, Gronostajowa 7a, 30–387 Krakow, Poland.
3 Microbiology Department, Faculty of Biochemistry, Biophysics and Biotechnology, Jagiellonian University, Gronostajowa 7, 30-387 Krakow, Poland.
4 Department of Organic Chemistry, Faculty of Chemistry, Nicolaus Copernicus University, 7 Gagarin Street, Torun, Poland
5 Shanghai Institute for Advanced Immunochemical Studies and School of Life Science and Technology, ShanghaiTech University, Shanghai, China
6 Dipartimento di Chimica e Chimica Industriale (DCCI) Università di Pisa Via Giuseppe Moruzzi, 13 - 56124 Pisa, Italy
7 Departamento de Quımica Organica, Universidade Federal Fluminense, Laboratorio de Sintese e Aplicaçao de Substancias Supramoleculares e Organocalcogenios (SupraSelen), Outeiro Sao Joao Batista s/n, 24020-141, Niteroi, RJ, Brazil
8 CNR-NANOTEC, SS Rende, Department of Physics, University of Calabria, Rende (CS) 87036, Italy
9 Institute of Biocomputation and Physics of Complex Systems, Joint Unit GBsC-CSIC-BIFI, University of Zaragoza, Zaragoza 50018, Spain

Keywords: Benzisoselenazolones, diselenides, SARS-CoV-2 main protease inhibitors, glutathione, Ebselen.

Abstract: Although global vaccination campaigns relieved the SARS-CoV-2 pandemic in terms of morbidity and mortality, the capability of the virus to originate mutants may reduce vaccines efficiency, posing a serious risk to fall into the pandemic again. As a result, there is the need to develop small molecules able to tackle conserved viral targets, such as the main protease (M^{pro}). Here a series of benzisoselenazolones and diselenides were tested for their ability to inhibit M^{pro}, then, for the most potent compounds, the antiviral activity was measured in vitro, and the mechanism of action was investigated. Density functional theory and molecular docking procedures were also implemented to shed a light into the protein/compound interaction. Finally, a bioorganic model was set up to investigate the reaction between selenorganic compounds and biologically relevant thiols, to unravel possible metabolic pathways of such compounds. The overall results contribute to identify a series of novel compounds active against SARS-CoV-2, and to clarify some important aspects in the mechanisms of action of Se-containing inhibitors targeting the SARS-CoV-2 main protease (M^{pro}).

Introduction:

The *Coronaviridae* family was first globally recognized as a public threat during the emergence of the severe acute respiratory syndrome (SARS) in 2003 [1] and, a decade later, its potential was confirmed by the emergence of the middle-east respiratory syndrome (MERS) [2]. Nonetheless, it was the unprecedented rapid emergence of SARS-CoV-2 and the resulting COVID-19 pandemic that triggered global research efforts to develop vaccines, therapeutics, and diagnostics to tackle this danger. While today effective vaccines are available, they do not prevent the infection and, in high-risk individuals, additional layers of protection are still desirable. Regrettably, despite the identification of several molecular targets of SARS-CoV-2 [3–5], the number of compounds required to drive an effective drug discovery program remains relatively limited compared to the undergoing efforts, with the majority of research focused on drug repurposing [6,7].

Main protease (M^{pro}) and papain-like protease (PL^{pro}) are two viral enzymes essential for virus replication and evasion of the host immune responses. The absence of closely related cellular homologs makes these enzymes particularly attractive targets for the design of coronavirus-specific antiviral agents. Among the first compounds to be discovered to block their enzymatic activity, the organoselenium compound 2-phenyl-1,2-benzoisoselenazol-3-one (ebselen, compound **1a**)[8,9] has been identified in a high-throughput screening study as a potent inhibitor of the main protease (M^{pro}),

within a pool of existing small-molecules [10]. Ebselen showed a potent inhibitory activity toward M^{pro}, with an IC_{50} in the high nanomolar range (670 nM) and inhibitory activity toward the infectious virus with an EC_{50} in the low micromolar range (4.67 μM)[10]. Subsequently, it was demonstrated that ebselen also inhibits the papain-like protease (PL^{pro}) from SARS-CoV-1 and SARS-CoV-2 (with an IC_{50}= 2.26 μM for PL^{pro} of SARS-CoV-2)[11]. The same authors of such pioneering study recently also reported a series of ebselen analogues as potent inhibitors of nsp14 guanine N7-methyltransferase [12]. Studies focusing on the identification of the mode of action of ebselen (**1a**) suggested that it acts as an irreversible inhibitor, covalently binding to the reactive cysteines in the PL^{pro} and M^{pro} active sites to form a stable selenyl sulfide. Tandem mass spectrometry and computational calculations proved that for SARS-CoV-2 the reactive cysteine of M^{pro} is Cys145 [4,13], whereas molecular modeling suggested that Cys111 is the target of Ebselen within the PL^{pro} active site [14]. In addition, molecular dynamics simulation suggested that, besides a covalent inhibition, ebselen may interact and inhibit M^{pro} also non-covalently by binding in a pocket localized between the II and the III domains of the protein [13].

The capability of ebselen to easily modify cysteines is well documented [15–19], and this could represent a major issue for its actual clinical exploitability. On the other hand, several studies demonstrated an almost complete absence of toxic effects *in vivo*, and this has also been proved by the clinical trials in which **1a** was evaluated [9,20]. Furthermore, from a general standpoint, ebselen shows several additional pharmacological effects that have been pointed out to be favorable in the context of curing COVID-19 [21].

Beside ebselen, a few others selenium-containing compounds endowed with anti-SARS-CoV-2 activity have been reported in literature (Figure 1).

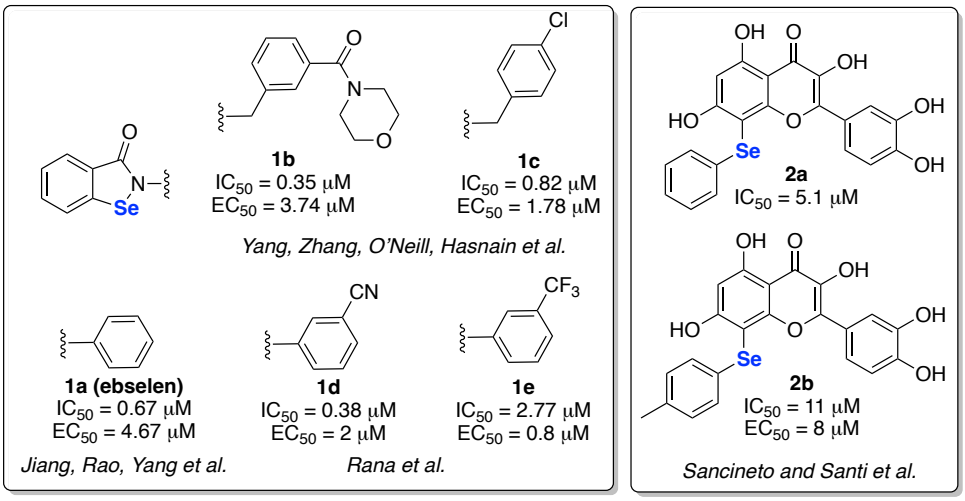

Figure 1. Se-containing compounds endowed with anti-M^{pro} and anti-SARS-CoV-2 activity. IC_{50} denotes the concentration at which enzyme activity is reduced by 50%; EC_{50} denotes the concentration at which the viral replication in Vero cells is reduced by 50%, as determined by RT-qPCR.

In particular, Yang, Zhang, O'Neill, and Hasnain tested a series of benzisoselenazolone analogs, previously reported as neuroprotective agents. They identified compounds **1b** and **1c** as being more active in inhibiting M^{pro} than **1a**. At the same time, in an attempt to resolve the co-crystal structure with the protein, the authors reported that these compounds were able to transfer a hydrogenselenide unit to Cys145 through a S_NAr-like reaction taking place in the M^{pro} active site [22]. A related study was carried out by Kumar *et al*., in which it was also proved the selenylation of the very same cysteine also by other benzisoselenazolones [23]. Recently, Rana *et al*. reported a series of ebselen close analogs with anti-M^{pro} activity, with compounds **1d** and **1e** being the best in class. These derivatives showed an improved anti-viral activity not only in Vero cells but also in other cell lines chosen because they better mirrored the lung epithelium [24]. Zhang, Wang, *et al.* recently reported benzisoselenazolones bearing different aromatics at the N2 positions. In the study, the authors identified compounds endowed with low nanomolar IC_{50} and antiviral activity in the micromolar range [25].

Besides benzisoselenazolones, selenides proved to be suitable substituents to improve the anti-SARS-CoV-2 activity of the natural product quercetin [26]. The resulting selenoquercetin analogs (**2a** and **2b)** demonstrated a striking ability to inhibit M^{pro}, with compound **2b** being active also *in vitro* at EC_{50} in the low micromolar range and without showing any cytotoxicity [27]. Recently also other selenides were reported by some of us as capable of inhibiting SARS-CoV-2 in a cellular context [28].

Taken together, these results clearly underline the value of selenorganic derivatives, in particular ebselen-like structures, as lead compounds to develop novel anti-SARS-CoV-2 compounds.

In light of this, we herein report the anti-SARS-CoV-2 properties of ebselen-like derivatives (compounds **1f-s**) and a series of closely related diselenides (compounds **3,4**). Considering that in studies reporting an anti-SARS-CoV-2 activity the ebselen core is always decorated with aromatic and benzylic substituents, we sought to prepare benzisoselenazolones bearing aliphatic side chains in order to enlarge the structure-activity relationship (SAR) features for this class of compounds. In addition, we provide mechanistic insight to prove that, for certain derivatives, a plausible metabolic link between benzisoselenazolones and the corresponding diselenides actually exists.

For the whole set of compounds herein reported, the anti-M^{pro} activity was initially assessed through an *in vitro* screening, and then mass spectrometry confirmed the covalent enzymatic inhibition. The most potent derivatives were then assayed in a cellular model of SARS-CoV-2 infection, by also investigating their mechanism of action. Not only benzisoselenazolones were found to be active, but also diselenides. A bioorganic, NMR-based model was purposely developed to get insight into the intracellular fate of the studied compounds.

Results and Discussion

Diphenyl diselenide (compound **8**) and selenocystine (compound **6**) are commercially available. Dibenzyl diselenide (compound **7**) was prepared following the procedure reported in literature [29]. Ebselen-like compounds **1f-1l** were prepared starting from **5** [29,30], which was first coupled with amino acids protected as esters leading to compound **3f, h-l** [31]. The ester derivatives were then converted into the corresponding benzisoselenazolone **1f-l**, following a procedure recently reported by some of us [32]. Diselenides having an acid moiety were obtained starting from the corresponding esters through mild basic hydrolysis, leading to compound **4f, h-l** (Scheme 1).

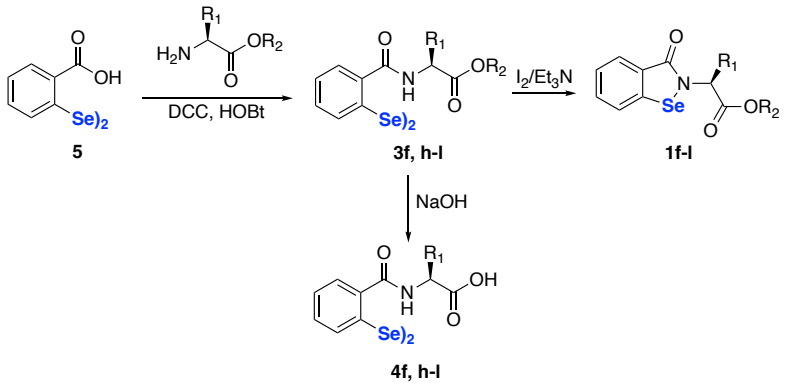

Scheme 1. Synthesis of diselenides **3,4** and benzisoselenenazolones **1f-l**. For R1 and R2 see Table 1. For synthetic details see references.[31,32]

Diselenides **3n-q, s** were prepared from the corresponding ebselen-like compounds (**1n-q, s**) [33] via a sequential $NaBH_4$-mediated reduction of the Se-N bond and air oxidation of the so-formed selenolate anion.[34]

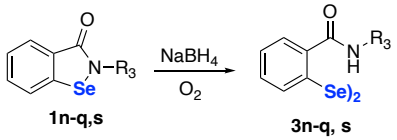

Scheme 2. Synthesis of diselenides **3n-q, s**.

As a first line of screening, the whole set of compounds was preliminarily assayed *in vitro* at the concentration of 40 μM, showing full inhibition of the enzymatic activity of M^{pro} (See Table S1). Then, the IC_{50} was determined, and the results are collected in Tables 1-3.

Table 1. Structures and IC_{50} values of all the Ebselen derivatives **1f-s**.

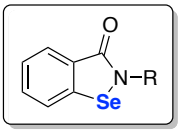

compound	R	IC_{50} nM	compound	R	IC_{50} nM	compound	R	IC_{50} nM
1f		201.4 ± 24.3	**1k**		56.30 ± 31.1	**1p**	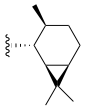	311.5 [a]
1g		166.8 ± 41.0	**1l**	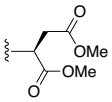	101.16 ± 97.4	**1q**	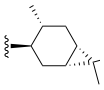	487.2 [a]
1h		149. 5 ± 18.1	**1m**		358.8 [a]	**1r**	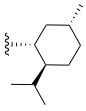	346.2 [a]
1i		87.64 ± 19.8	**1n**		334.9 [a]	**1s**		203.2 [a]
1j	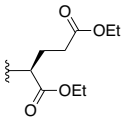	101.5 ± 39.5	**1o**		518.9 [a]			

a) acquired as a single experiment.

Table 2. Structures and IC_{50} values of diselenides **3f**, **3h-s**; **4f**, **4h-i**.

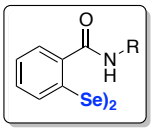

compound	R	IC_{50} µM	compound	R	IC_{50} µM	compound	R	IC_{50} µM
3f		0.56 ± 0.21	**3j**	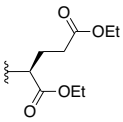	6.28 ± 4.04	**3n**		ND
4f		6.49 ± 1.36	**4j**	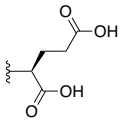	> 100	**3o**		6.133 [a]
3h		1.06 ± 0.23	**3k**		1.39 ± 0.09	**3p**	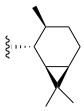	3.449 [a]
4h		5.44 ± 1.86	**4k**		4.87 ± 2.97	**3q**	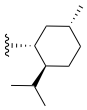	8.332 [a]
3i		1.26 ± 0.36	**3l**	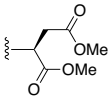	1.92 ± 0.68	**3s**		43.16 [a]
4i		5.14 ± 2.39	**4l**	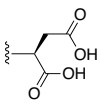	11.84 ± 2.48			

a) acquired as a single experiment

Table 3. Structures and IC_{50} values of other diselenides (**5-8**).

compound		IC_{50} µM	compound		IC_{50} µM
5	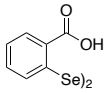	ND	**7**	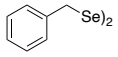	ND
6	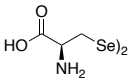	64.86 [a]	**8**		1.87 ± 0.26

a) acquired as a single experiment; ND not determined.

The ebselen derivatives (**1f-s**) were generally more potent than the corresponding diselenides **3f-s** and **4f-l**. Derivatives **1k** and **1i** were the best in class among the compounds tested, with an IC_{50} in the low nanomolar range. In all the cases, an anti-M^{pro} activity higher than that of ebselen and most of its derivatives reported in the literature was observed, highlighting that the replacement of the aromatic ring with an aliphatic one improves the ability to bind and inhibit the viral protease. Terpenes-containing derivatives **1m-s** displayed activity in the high nanomolar range.

Regarding the diselenides, compounds **5** and **7** were unable to exert any sort of inhibition, whereas selenocystine (compound **6**) had an IC_{50} in the high micromolar range. Surprisingly, also diphenyl diselenide **8** showed a low micromolar activity. The introduction of a carboxamide substituent in the *ortho* position with respect to the selenium atom preserved or even improved the activity, as in the case of compound **3f**. From the comparison among compounds containing an ester functionality (**3h-l**) with the ones containing an acid moiety (**4h-l**), it clearly emerged that the latter were less active in the M^{pro} inhibition. Again, the terpene derivatives **3p-q** and **3s** were able to inhibit M^{pro}, but they required a higher concentration compared to the other compounds, and compound **3n** was completely inactive.

The better activity of ebselen-derivatives in comparison with the diselenides could be ascribed to a higher electrophilicity of the former, which facilitates the reaction with reactive thiols and, as a consequence, the covalent inhibition of the protein. The greater electron deficiency of ebselen derivatives can be clearly deduced from the chemical nature of the two functional groups (a selenazolone and a diselenide) and is also confirmed spectroscopically by comparison of their ^{77}Se NMR chemical shifts, ranging from 804 to 935 ppm for benzisoselenazolones and from 439 to 450 ppm for the diselenides.

As a further evaluation of the electrophilicity of these compounds, the geometry of some selected ebselen-like and diselenides systems was optimized by DFT (b3lyp-d3/def2-tzvp level of theory), and the natural partial atomic charges were computed by using the Natural Population Analysis (NPA) as implemented in the NBO software suite. The results are shown in Table 4.

Table 4. NPA partial charge (in *e*) on the selenium atom (two values are shown for diselenide systems) on some ebselen-like and diselenides systems.

compound	q(Se)	compound	q(Se)
1a	0.607	**3k**	0.165/0.167
1f	0.613	**3p**	0.143/0.175
1i	0.619	**5**	0.173/0.186
1k	0.617	**6**	0.104/0.122
1p	0.608	**8**	0.151/0.153

The q(Se) value resulted to be inversely proportional to the IC_{50} value; compounds having q(Se) > 0.610 *e* are the most active. This observation further supports the hypothesis of a nucleophilic attack of the sulfur of the cysteine to the selenium as a key step in the inhibition process in the tests in vitro. Noteworthy, some diselenides show an asymmetric charge distribution among the two selenium atoms. This is a consequence of a non-symmetrical involvement of the selenium atoms in weak interactions with the nearby chemical environment (Figure S1). For example, in **3p** only one selenium is involved in two hydrogen bonds with the two amide groups, producing a slight polarization of the Se-Se bond.

Molecular docking was also used as an additional computational tool to investigate the binding of selected ligands in the active site of M^{pro}, and the steric constraints that may limit their access to the binding pocket. In particular, we focused on **1a** (ebselen), **1i**, and **1r**, as representative examples of compounds with subtle structural difference leading to appreciable variations among their IC_{50} values (see Table 1 and data reported in literature for **1a**[10]). The results reported in Table 5 show that these compounds have a good affinity towards the binding site of M^{pro}, with docking scores of at least –6 kcal/mol, which is comparable with values previously found for other experimentally-validated binders of this protein.[26,35] The differences among the three compounds tested were negligible within the limit of the accuracy (about ±0.3 kcal/mol) in the scoring function of the docking algorithm.[36] This finding suggests that the activity in the high nanomolar range observed for **1r**, and in common with the other terpenes-containing derivatives, should not be ascribed to steric clashes within the binding site. We also observed that the affinities of these compounds did not change significantly by considering as flexible the side chains of protein residues His41/Cys145, indicating that rearrangements of the catalytic dyad of M^{pro} do not play an essential role in the binding.

In the docking poses, the minimum non-bonding distance found between the sulfur atom of Cys145 and the selenium was ~ 3.7 Å, as it could be expected considering their van der Waals radii (1.8 and 1.9 Å, respectively). However, we also verified (see Methods section) that each compound is able to form a covalent bond Se–S (with a distance < 2.5 Å) and still fit within the active site of M^{pro} without requiring a local reorganization of the protein pocket. Therefore, although docking simulations cannot

predict the fate of the molecular structure of these compounds, still they cannot exclude that it might be intact until the formation of the covalent bond Se–S.

Table 5. Affinity (calculated considering the catalytic dyad His41/Cys145 in the binding pocket either as rigid or flexible) and minimum non-bonding distance between Se and S atoms observed in molecular docking for selected ebselen-like compounds.

compound	Affinity (kcal/mol) [rigid dyad]	Affinity (kcal/mol) [flexible dyad]	Minimum distance (Å) [Se···S]
1a	–6.142	–6.256	3.766
1i	–5.938	–6.290	3.606
1r	–6.351	–6.597	3.734

We then evaluated whether the anti-M^{pro} activity of the most potent compounds translate into the inhibition of the SARS-CoV-2 replication. The selected compounds were glycine derivatives **1f**, **1g, 3f,** and **4f**, isoleucine derivatives **1i** and **3i**, valine derivatives **1k**, **3k,** and **4k**, and benzisoselenazolones containing glutamic and aspartic esters **1j** and **1k**. Ebselen **1a** was tested in parallel as a positive control. First, the cytotoxicity was evaluated at 100, 80, 60, 40, 20 μM concentration in Vero cells. No toxicity was recorded for all compounds except for **3f** that that was highly toxic at 100 μM (Figure S2). Next, confluent monolayers of Vero cells were infected with the virus in the presence or absence of the inhibitors. All compounds were tested at 100, 80, 60, 40, and 20 μM concentration (except for **3f**, which was not tested at 100 μM). 2 days post-infection, the cytopathic effect was assessed, and toxicity for **1f**, **1l**, **3i** was observed at 100 μM and for **1g** at 100 and 80 μM**,** therefore these conditions were not collected for further analysis. Cytotoxicity for some compounds observed in infected cells as compared to XTT assay could be due to cellular stress caused by viral infection. All remaining samples were harvested and evaluated by means of quantitative PCR coupled with reverse transcription (RT-qPCR) (Figure S3). The EC_{50} values were determined as summarized in Table 6, with the exception of compound **4f** which was inactive. All compounds inhibited viral replication at low micromolar levels, with the ebselen-like compounds **1j** and **1l** endowed with the lowest, and mutually similar, EC_{50} (7 and 8 μM, respectively). From a SAR standpoint, the double ester functionality seems to improve the antiviral activity of the compounds. The similarity of the EC_{50} of the two compounds mirrors their activity toward the Mpro, against which they showed comparable potencies (see Table 1 and 6). Compound **1i**, which is a nanomolar M^{pro} inhibitor, inhibits the viral replication with remarkable activity. Unexpectedly, the most potent M^{pro} inhibitor, **1k**, exerted an antiviral activity lower than expected on the basis of the biochemical assay. Among diselenides, the esters were way more potent than acids (see data for **3f** *vs* **4f**, and **3k** *vs* **4k**), regardless of their side chain.

Table 6. EC_{50} values of the tested compounds.[a]

compound	EC_{50} (μM)
1a	12
1f	24
1g	15
1i	11
1j	8
1k	24
1l	7
3f	21.3
3i	11
3k	15
4f[b]	>100
4k	32

[a]Compounds **1a**, **1i**, **1j**, **1k**, **3k** and **4k** were devoid of any toxicity up to 100 μM, compounds **1f**, **1l**, **3f** and **3i** up to 80 μM and compound **1g** up to 60 μM; [b]inactive in antiviral assay up to 100μM

Time of addition (TOA) experiments were also carried out to map the mode of action of the compounds. The most promising ebselen-like derivatives **1i** and **1l**, and diselenides **3i** and **3k**, together with **1a**, were added at three different stages of virus infection at a concentration of 60 μM.

Assay I (PRE) was used to assess whether the compounds may render the cells resistant to the virus. As such, they were added before infection and cells were pre-incubated with compounds for 1 h at 37°C. Assay II (WITH) was to verify whether the compounds affect viral entry (i.e., early stages of replication). Thus, they were added with the virus, during the infection. Finally, the assay III (POST) in which compounds were added 2 h after infection was performed to assess their impact on viral replication and egress (i.e., late stages of replication).

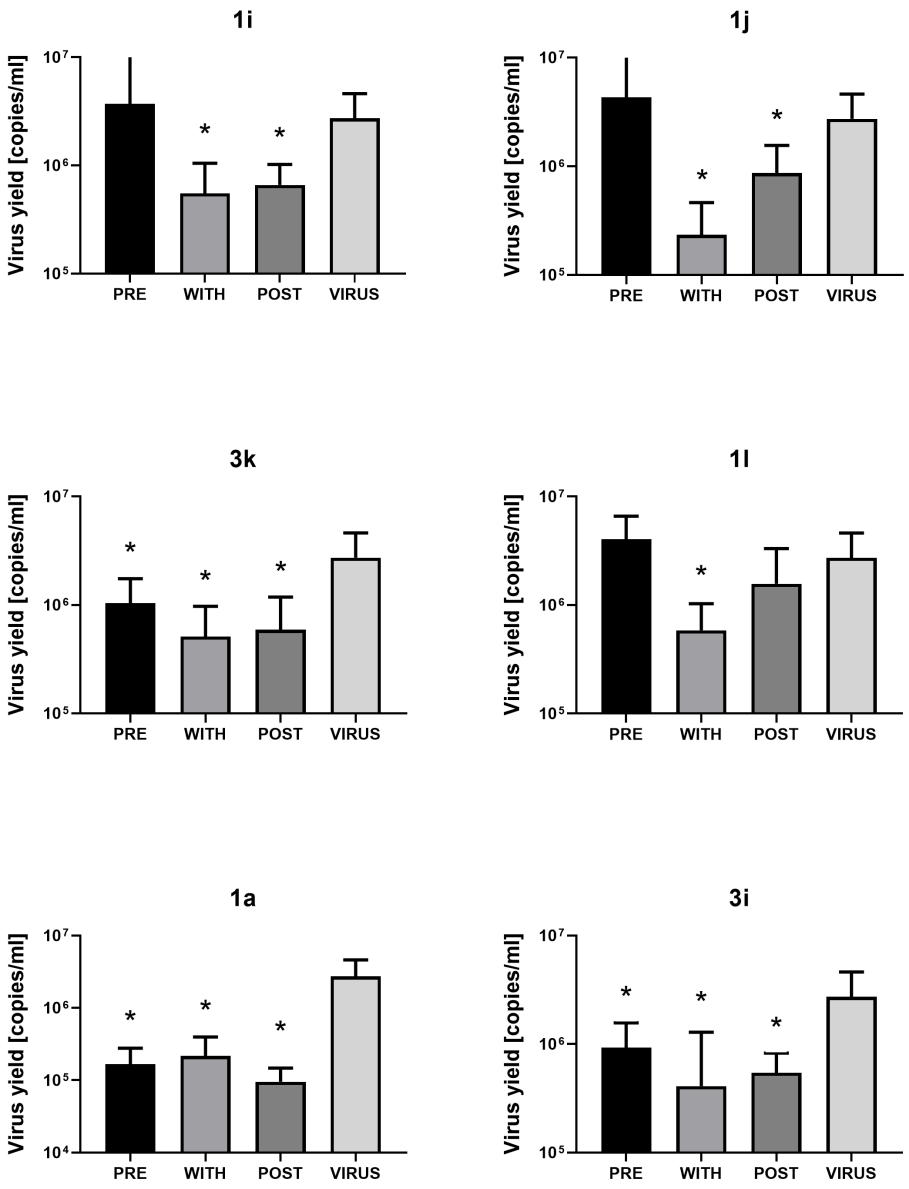

Figure 2. TOA experiments for selected compounds. The inhibition of virus replication in Vero cells by tested compounds added at different times of infection (PRE, WITH and POST – see main text for description). The figure shows qRT-PCR analysis of cell culture supernatants infected with SARS-CoV-2 at $TCID_{50}$ of 1,600 per mL) 12 h post-infection. All the experiments were performed in triplicate, and the results are presented as averages, with error bars denoting Standard Error of the Mean (SEM). To determine the significance of the obtained results, Kruskal-Wallis multiple comparisons test was performed. P values of < .33 (*); <.002 (**); <.001 (***) were considered significant.

As shown in Figure 2, the compounds **1i**, **1j,** and **1l** inhibited the SARS-CoV-2 virus at the early and late stages of the infection. We did not observe any effect of preincubation of cells or virions, suggesting that the inhibition occurs during the virus entry and replication. In the case of compounds **3i**, **3k**, and for ebselen (**1a**) used as a control**,** inhibition was observed at multiple stages, including in the pre-incubation assay, suggesting a different mechanism of action or an intracellular accumulation of the compounds. Conversely, the lack of activity of ebselen-like compounds **1i**, **1j,** and **1l** could derive from their

reaction/interaction with cellular thiols different from Cys145 of M^{pro}. Such a reaction would convert the compounds into their selenylsulfide analogs, whose activity against the viral protease remains to be proven.

The electrophilic reaction of selenium-containing compounds with nucleophilic thiols is a well-known process [37], and this pro-oxidant property should explain why some of them are toxic. Among the thiols, glutathione (GSH) is the most abundant in living cells, especially under oxidative stress conditions [38]. For this reason, a direct interaction between every electrophilic selenium-containing compound and GSH may be considered as the first chemical event that involves them in the cellular environment. With the aim to improve our understanding of this topic, we set up an NMR-based model meant to study the reaction/interaction between selected compounds and GSH. In particular, beside an ^{1}H-NMR analysis, we selected the ^{77}Se NMR that represents an ease and reliable method to identify organoselenium derivatives in non-purified reactions mixtures directly performed in an NMR tube [39]. Unfortunately, limits associated with sensitivity and relaxation time hampered a quantitative interpretation of the obtained results.

The poor solubility of ebselen and its derivatives in buffered aqueous conditions forced us to select DMSO-d_6 as solvent for the reaction, even though it could not be considered totally inert based on its mild oxidant properties.

As reported by Back and coworkers, one molar equivalent of reduced glutathione rapidly converts **1** into **9** (Scheme 3) [40]. It is also known that the second equivalent of reductant (GSH) promotes the rapid and quantitative formation of the corresponding diselenide **3a**. We demonstrated that this latter transformation can be activated by 5 mol % of starting from **9** and leading to the formation of diselenide **3a** and oxidized glutathione in up to 50% conversion, accounting for a self-catalytic process according to the equilibrium depicted in Scheme 3 (Figure S4).

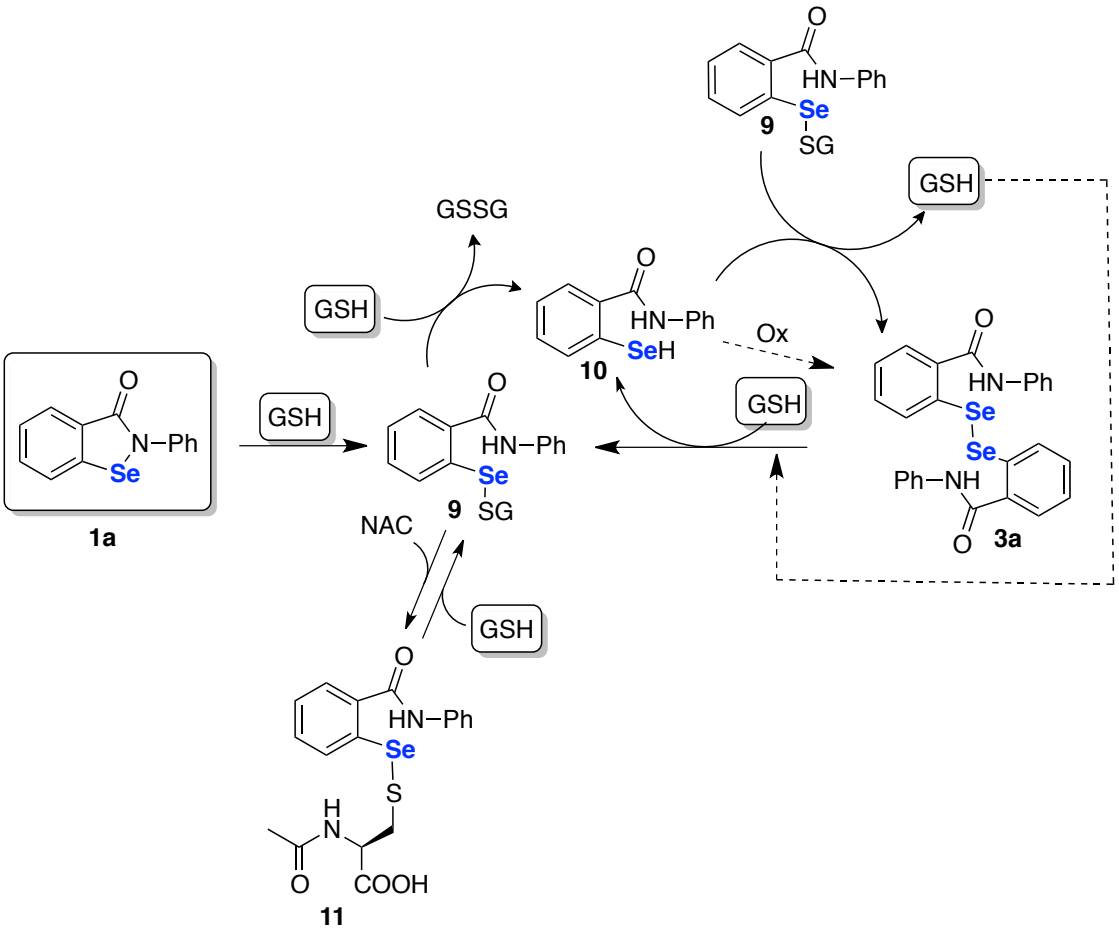

Scheme 3. Fate of Ebselen **1a** and the corresponding diselenide **3a** in the presence of GSH.

Diselenide **3a**, synthesized according to literature [11], was analyzed by means of ^{77}Se NMR in DMSO-d6 and a peak at 442 ppm was observed. By the addition of a one molar equivalent of GSH, the signal of selenylsulfide **9** at 547 ppm appeared. Not all the diselenide was consumed in the reaction, indicating that the reaction with GSH is not as fast as that involving compound **1** (Figure S5). Diselenide **3k** was subjected to the same investigations, showing a behavior similar to that of the derivative **3a** (Figure S6).

Two things emerge clearly from the proposed mechanism: 1) under reducing conditions Ebselen **1a** cannot be considered as the final chemical entity responsible for the interaction with M^{pro} 2) both Ebselen **1a** and the corresponding diselenide **3a** in the presence of a reducing thiol establish an equilibrium between **9**, **10** and **3a**, that it was demonstrated to be prone to further thiol exchange processes. When this mixture was reacted with N-acetylcysteine (NAC), ^{77}Se NMR showed the formation of another compound having a chemical shift compatible with that of the selenylsulfide **11** (Figure S7). This indicate that the above-described equilibria can be further modulated by thiol exchange processes.

These data suggest that a particular attention should be paid in the interpretation of the data produced by the enzymatic inhibition test. In fact, when it is performed under non-reducing conditions, it may not be able to correctly interpret the molecular mechanism and consider the molecular species actually involved in a real biological environment, losing its predictability.

For this reasons, freshly prepared compounds **1a** and **3a** were assayed in parallel against M^{pro} both in the presence and absence of DTT (as a reducing thiol). The results are summarized in Table 7.

Table 7. anti Mpro activity of **1a** and **3a**

compound	IC_{50}
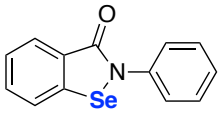 **1a**	36 nM[a] 432 μM[b]
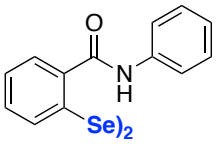 **3a**	65 nM[a] 209.46 μM[b]

[a]Tested in the absence of DTT; [b]tested in the presence of DTT.

As also reported by Wang[41], the anti M^{pro} activity of **1a** drops dramatically in the presence of DTT, and this is also true for diselenide **3a**, that, in the presence of the reducing agent, displays an IC_{50} in the high micromolar range. As expected, in the absence of a reducing agent, ebselen is more potent that its diselenide, mirroring the higher electrophilicity of the selenium atom. In the presence of DTT, both **1a** and **3a** produced the same effect in terms of IC_{50} (considering that **3a** is a dimer), in accordance with the mechanism proposed in Scheme 3.

Clearly, this mechanism require that that Se-Se bond should be polarized. As an example, glutathione is not able to reduce diphenyl diselenide **8** even when used in a large excess. In our cases, the amide functionality adjacent to the selenium atom can establish a non-bonded interaction able to modulate the electrophilicity and the redox properties of the selenium atom. This underlines that probably not all the diselenides (and not all the ebselen-derivatives) share the same reactivity and mechanism in the enzyme inhibition. Beside the covalent inhibition, a non-covalent mechanism of action can reasonably be speculated for some of them. This is the case of compound **8**, which is still able to inhibit M^{pro}, but thought a non-covalent mechanism as recently proposed by Orian and Rocha.[42]

HRMS analysis performed under reducing conditions (for the presence of DTT, see SI) evidenced that both selenazolones and diselenides bind covalently the M^{pro}, but not in the same manner and not selectively. The mass of apo M^{pro} is ~33.8 kDa, in line with previous observations.[10] In experiments with ebselen **1a**, and the analogous **1i**, **1l**, and **1k**, a mass corresponding to M^{pro} in covalent complexes with one, two, or three intact molecules was observed. In contrast, **3a** and **3i**, afforded peaks corresponding to M^{pro} in covalent complexes with one, two, or three halves of the intact compounds. In the case of **1j**, the increase in M^{pro} mass did not correspond to either the intact molecule or half of it. Finally, **3k** did not produced relevant covalent modification of M^{pro}.

To rule out that the inhibition could arise from compound **9**, we tested by molecular docking simulations whether it could sterically bind within the active site of M^{pro}, but the results suggest that the GSH moiety would remain solvent-exposed, and sterically hamper the anchoring of the compound with the selenium in a position favorable to form a covalent bond with Cys145. This finding is coherent to the observations recently reported by Teixeira da Rocha [43].

Finally, as a further investigation of the mechanism showed by those compounds that were proved to inhibit viral replication when administered before virus addition, an entry inhibition assay was set up. Compounds **1a**, **3i,** and **3k** were tested for their ability to inhibit the spike (S) protein-mediated internalization of pseudoviruses, using the VSV-G-glycoprotein-decorated pseudoviruses as control. Such a system allows one for the identification of a direct interference with the entry process and the assessment of the selectivity of this process. As shown in Figure 3, compound **1a** showed the ability to block the entry of both pseudoviruses when tested at 60 μM, indicating that it interferes with the viral entry process in an unspecific manner. In contrast, compounds **3i** and **3k** did not inhibit the entry of the pseudoviruses.

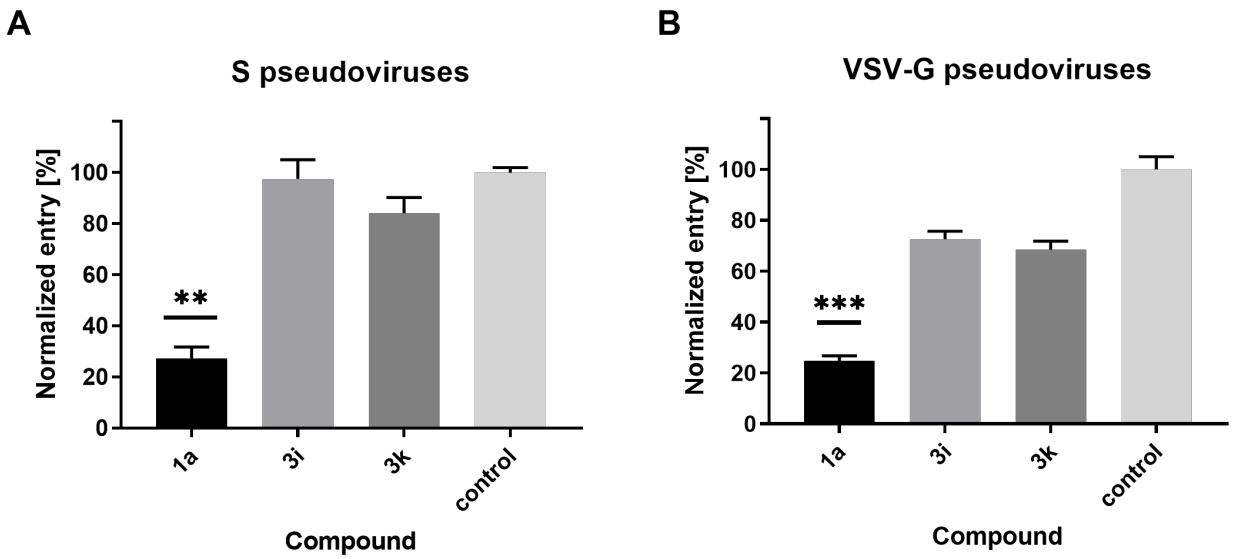

Figure 3. Inhibition of SARS-CoV-2 pseudovirus entry. The inhibition of SARS-COV-2-S (A) or control VSV-G (B) pseudovirus (positive control) entry to $HeLa^{ACE2+}$ cells by **1a**, **3i**, and **3k** compounds at 60 μM concentration. The figure shows normalized signal from cell culture lysates collected 72 h post-inoculation. All the experiments were performed in triplicate, and the results are presented with standard deviations (SD) error bars. The data were normalized to untreated transduced control which was arbitrary set at 100%; Kruskal-Wallis multiple comparisons test was performed to assess the significance of obtained results. P values of < .33 (*); <.002 (**); <.001 (***) were considered significant.

Conclusion:

From the screening of some benzisoselenazolones and diselenide analogues, a series of new M^{pro} inhibitors has been identified. Computational investigations proved that the inhibition is likely covalent with a direct proportionality between the IC_{50} and the electrophilicity of selenium among the tested compounds. Most of the M^{pro} inhibitors are endowed with antiviral activity measured in a cell context without major cytotoxicity, thus leading to positive selectivity index values, even if the non-specific activity of selenium compounds is well-described and reported in several cases[41,44–46]. Time of addition studies proved that, although the antiviral potency (expressed in terms of EC_{50} values) is similar among the compounds, differences are still present. Ebselen, as an example, is able to inhibit viral replication when added either pre-, with- and post–infection, whereas benzisoselenazolones **1i**, **1j** and **1l** are devoid of any activity when the administered virus is added to the cells. This indicates that minor structural variations in these compounds have an impact on their specific antiviral properties, but not in their overall ability to cause an M^{pro} inhibition.

We have also demonstrated that the antiviral activity cannot be traced back in a simplistic manner to the direct interaction of benzisoselenazolones with residue Cys145 of M^{pro}. Its marked electrophilicity leads it to react rapidly and quantitatively with glutathione, most likely leading to a mixture in which the glutathionated adduct is in a dynamic equilibrium with the corresponding selenol and diselenide. This equilibrium can be obtained also starting from the diselenide, and it is prone to further modulation thought thiol exchange processes that could be envisioned as those responsible for the non-selective selenenylation of different free cysteine of the enzyme. Furthermore, it was demonstrated that ebselen also acts by inhibiting the spike (S) protein-mediated internalization of pseudoviruses, depicting a multifaced non-selective mechanism of action that involves both benzisoselenazolone derivatives and the corresponding diselenides. A more generalist approach is therefore necessary in the interpretation of the mechanism of action of these derivatives, and any reductionist simplification may miss important details of their functioning.

Experimental Section

DFT studies

All the geometry optimizations were performed with the Orca code[47], version 4.1.0 at the B3LYP/def2-TZVP level and def2/J auxiliary basis. Dispersion effects were taken into account using the Grimme D3-parametrized empirical dispersion correction, with the Becke–Johnson (BJ) damping function[48,49]. Frequency calculations were carried out at the same level of theory, to ensure that the

stationary structures had no imaginary frequencies. The solvent effects were modelled using the Conductor-Like Polarizable Continuum Model (CPCM), with water as solvent.
NBO atomic charges has been computed using the NBO6 suite of software[50].

Molecular docking

Molecular docking was performed by using AutoDock Vina, version 1.2.3 [36], following a protocol already used to test the binding of other ligands to the main protease of SARS-CoV-2 [35,51]. The structure of M^{pro} was taken from the crystal conformation of the ligand-free enzyme (Protein Data Bank entry: 6Y2E [52]), and considered either fully rigid or partly flexible in the sole side chains of the catalytic dyad His41/Cys145. Compounds **1a**, **1i**, and **1r**, simulated as representative examples of ebselen-like ligands, were built by using the molecular editor Avogadro, version 1.2.0 [53], and full flexibility was allowed for rotations around their dihedral angles. The binding of Se-GSH to the active site was also probed in the same way. In all cases, a blind search was carried out within a volume encompassing the whole protein, and with an exhaustiveness 16 times larger than the default value [54].

Additional simulations were run to test whether compounds **1a**, **1i**, and **1r** could be covalently bond with the catalytic Cys145 without requiring a structural reorganization of the active site of M^{pro}. In this case, M^{pro} was built from the complex with an ebselen-derivative inhibitor (Protein Data Bank entry: 7W9G [54]), in which the sole coordinates of the selenium atoms bound to S-Cys145 are reported. Since AutoDock Vina is not able to simulate a covalent docking, each of our compounds was modeled as an adduct already bound to the (modified) residue Cys145, and with the same C^{α}–S–Se geometry present in the crystallographic structure. Afterwards, the self-docking of the fully-flexible side chain of such Cys-modified residue and the rest of the rigid protein structure was simulated. The existence of bound conformations of the compounds that fit into the protein active site was verified by visual inspection, as well as by binding affinities (< –15 kcal/mol) incompatible with extensive steric clashes (which would lead instead to large positive values).

Chemistry

Compound **6** and **8** were purchased from Sigma Aldrich and used without further purifications. Compounds **1a**, **1f-1l** were prepared as we previously reported in Nascimento *et al.* [32], compound **3a** was prepared as reported in Weglarz-Tomczak *et al.* [11], compounds **3f**, **3h-3l**, **4f**, **4h-4l** and **5** were prepared as reported in Sancineto *et al.* [31]. Compound **7** was prepared as reported in Krasowska *et al.* [29]. Diselenides **3n-q, s** were prepared from the corresponding ebselen-like compounds (**1n-q, s**) [33] via a sequential $NaBH_4$-mediated reduction of the Se-N bond and air oxidation of the so-formed selenolate anion [34]. Spectral data are superimposable to those reported in literature.

NMR experiments

NMR experiments were carried out at 25 °C on a Bruker Avance NEO 600 MHz spectrometer equipped with Cryoprobe Prodigy and operating at 600 MHz for ^{1}H, and 114.45 MHz for ^{77}Se experiments. ^{1}H, and ^{77}Se chemical shifts (δ) are reported in parts per million (ppm) and they are relative to TMS 0.0 ppm and the residual solvent peak of DMSO-d6 at δ 2.35 ppm. ^{77}Se experiments were referenced to $PhSe_2$ (^{77}Se δ = 463 ppm in $CDCl_3$).

For the experiments reported in Figure S4, a solution of compound **9** (21 mg, 0.036 mmol), prepared as reported in Sands *et al.* [40], in 1 ml of DMSO-d6 was prepared, then 0.0018 mmol of GSH (from a 0.4 M stock solution in D_2O) were added. Sequential ^{1}H and ^{77}Se NMR spectra were recorded.

For the experiment reported in Figure S5, a solution of compound **3a** (10 mg, 0.018 mmol) in 1 ml of DMSO-d6 was prepared, then a stoichiometric amount of GSH (0.018 mmol from the above-mentioned stock solution) was added. Sequential ^{1}H and ^{77}Se NMR spectra were recorded.

For the experiment reported in Figure S6, a solution of **3k** (12 mg, 0.018 mmol) in 1 ml of DMSO-d6 was prepared, then a stoichiometric amount of GSH (0.018 mmol from the above-mentioned stock solution) was added. Sequential ^{1}H and ^{77}Se NMR spectra were recorded.

For the experiment of Figure S7, a solution of **1a** (5.1 mg, 0.018 mmol) in 1 ml of DMSO-d6 was prepared, then a stoichiometric amount of GSH (0.018 mmol from the above-mentioned stock solution) was added. Sequential ^{1}H and ^{77}Se NMR spectra were recorded. To the same sample, a stoichiometric amount of N-acetyl cysteine (NAC, from a 0.4 M stock solution in D_2O) was then added. Sequential ^{1}H and ^{77}Se NMR spectra were recorded to reveal the formation of a 1:1 mixture of two selenylsulfides **9** and **11**. To the same sample, 0.018 mmol of GSH was later added, sequential ^{1}H and ^{77}Se NMR spectra were recorded, and a higher amount of **9** was observed as revealed by the heights of the ^{77}Se resonance peak. Finally, to the same sample, 0.036 mmol of NAC was added, and a higher amount of **11** was observed as revealed by the heights of the ^{77}Se resonance peak.

Cells and viruses

Vero cells (Cercopithecus aethiops; kidney epithelial; ATCC CCL-81) and HeLa cells overexpressing ACE2 ($HeLa^{ACE2}$) cells were maintained in Dulbecco-modified Eagle's medium (DMEM, high glucose, ThermoFisher Scientific, Poland) supplemented with 5% heat-inactivated fetal bovine serum (FBS, ThermoFisher Scientific, Poland). The medium was supplemented with penicillin (100 U/mL, ThermoFisher Scientific, Poland) and streptomycin (100 µg/ml, ThermoFisher Scientific, Poland). Cells were cultured at 37°C in an atmosphere containing 5% CO_2 and humidity. Every two weeks, cells were tested for mycoplasma contamination.

Reference SARS-CoV-2 strain 026V-03883 was kindly granted by Christian Drosten, Charité—Universitätsmedizin, Berlin, Germany, by the European Virus Archive—Global (EVAg); https://www.european-virus-archive.com/, accessed on 15 April 2021).

SARS-CoV-2 stock was generated by infecting monolayers of Vero cells. The cells were incubated at 37°C under 5% CO_2. The virus-containing medium was collected at day 2 post-infection (p.i.), aliquoted, and stored at -80°C. Control samples from mock-infected cells were prepared in the same manner.

Virus yields were assessed by titration on fully confluent cells in 96-well plates according to the method of Reed and Muench.[55] Plates were incubated at 37°C, and the cytopathic effect (CPE) was scored by observation under an inverted microscope.

Time of addition assay

To discover the mechanism of action of the tested compounds, the inhibitors were added at three different stages of virus infection: PRE – compounds were added before infection, and cells were pre-incubated with compounds for 1 h at 37°C; WITH – compounds were added to the virus, during the infection; POST – compounds were added after infection (2 h post-infection). In details, the Vero cells were seeded in a culture medium on a 96-well plate 1 day before infection. Fully confluent cells were inoculated with 1600 $TCID_{50}$/ml of the SARS-CoV-2 virus, either in the presence or absence of the inhibitors. Mock control and medium control were also included. Cells were then incubated for 2 h at 37°C and 5% CO_2. Afterward, the cells were washed twice with PBS. Only in the POST-treatment version, each compound was applied into the cells monolayer, whereas in other conditions (PRE and WITH) the medium was applied into the cells monolayer. Cell culture supernatants were collected after 24 h for viral RNA isolation. The SARS-CoV-2 experiment was performed in triplicate biological and technical replications.

Pseudoviruses experiments

To verify the activity of the tested compound on PRE infection step, the assay with pseudoviruses was conducted. Briefly, $HeLa^{ACE2}$ cells were seeded in 96-well plates, cultured for 24 h at 37°C with 5% CO_2, and pre-incubated with tested compounds (60 μM) for 30 min at 37°C and then transduced with pseudoviruses harboring VSV-G or S-SARS-CoV-2 proteins or lacking the fusion protein (ΔEnv) in the presence of polybrene (4 mg/ml, Sigma-Aldrich, Poland). After 4 h of incubation at 37°C, unbound virions were removed by three washes with PBS, and cells were further cultured for 72 h at 37°C with 5% CO2. Cells were lysed in Bright-Glo luciferase assay buffer (Promega, Poland) and transferred onto white 96-well plates. Luminescence levels were measured on SpectraMax iD5 Multi-Mode Microplate Reader (Molecular Devices, San Jose, CA, USA).

Isolation of Nucleic Acids, Reverse Transcription, and Quantitative PCR

A viral DNA/RNA kit (A&A Biotechnology, Gdansk, Poland) was used for nucleic acid isolation from cell culture supernatants. RNA was isolated according to the manufacturer's instructions. Viral RNA was quantified using quantitative PCR coupled with reverse transcription (RT-qPCR) (GoTaq Probe 1-Step RT-qPCR System, Promega, Poland) using a CFX96 Touch real-time PCR detection system (Bio-Rad, Munich, Germany). The reaction was carried out in the presence of the probes and primers (Fwd: CAC ATT GGC ACC CGC AAT C; Rev: GAG GAA CGA GAA GAG GCT TG; probe: 6FAM-ACT TCC TCA AGG AAC AAC ATT GCC A-BHQ-1). The heating scheme was as follows: 15 min at 45 °C and 2 min at 95 °C, followed by 40 cycles of 15 s at 95 °C and 1 min at either 58 °C or 60 °C. In order to assess the copy number of the N gene, standards were prepared. The PCR product was amplified and cloned into pTZ57R/T plasmids using an InsTAclone PCR cloning kit (Thermo Scientific). The resulting plasmid was linearized, and its concentration was assessed using a NanoDrop™ 2000 spectrophotometer (Thermo Fisher Scientific, Waltham, MA, USA); the number of copies was deducted based on the Avogadro constant. Eight 10-fold serial dilutions were used as a qPCR template to develop a standard curve.

Statistical Analyses

The results are expressed as mean ± standard error of the mean (SEM). The statistical significance of the data presented in the manuscript was assessed with the non-parametric Kruskal–Wallis test, and P values below 0.05 were considered significant unless stated otherwise. Statistical analysis was performed using GraphPad Prism 9 (GraphPad Software Inc., San Diego, CA). For the determination of the half-maximal inhibitory concentration (IC_{50}), a dose–response curve fit was performed by using a nonlinear regression model.

Author Contributions: Conceptualization, JK, JS, YL, KP, CS; methodology, AD, JK, JS, YL, CS; formal analysis, LS, FM, AD, CSc, VC, JK, GC, BR, AK-P, JL; investigation, LS, FM, AD, AJP, MOF, CSc, VC, JK, YZ, GC, VN, BR, AK-P, YL; data curation, LS, JK, GC, YL, KP; resources, JK, JS,YL, KP, CS; software, GC, BR; writing original draft preparation, LS, JK, GC, CS; writing review and editing, LS, AD, JK, GC, BR, AK-P, HY, YL, KP, CS; visualization, LS; supervision, JK, CS, YK, KP, CS; funding acquisition, JS, YL, KP, CS. All authors have read and agreed to the published version of the manuscript.

Acknowledgments: This work was undertaken under the umbrella of the Selenium Sulfur Redox & Catalysis Network (SeSRedCat).

Funding: (CS**)** This research was supported by Department of Pharmaceutical Sciences with the project DELPHI "Dipartimenti di Eccellenza 2023-2027" and by University of Perugia with project "Ri-cerca di Base".

(KP) This work was supported by the DURABLE project, co-funded by the European Union, under the EU4Health Programme (EU4H) (https://health.ec.europa.eu/funding/eu4health-programme-2021-2027-vision-healthiereuropean-union_en#work-programmes), and ERAnet ICRAD—project Musecov: Multiscale Eco-evolution of Coronaviruses: from surveillance toward emergence prediction (https://www.era-learn.eu/network-information/networks/icrad/1st-icrad-call-2019/multiscale-eco-evolution-of-coronaviruses-from-surveillance-toward-emergence-prediction)

Institutional Review Board Statement: Not applicable.

Informed Consent Statement: Not applicable.

Data Availability Statement: All the data are within this manuscript and the supporting infor-mation "Further details are available under reasonable request"

Conflicts of Interest: The authors declare no conflict of interest.

References:

1. Peiris, J. S. M., Guan, Y. & Yuen, K. Y. Severe acute respiratory syndrome. *Nat. Med.* **10**, S88–S97 (2004).
2. Memish, Z. A., Perlman, S., Van Kerkhove, M. D. & Zumla, A. Middle East respiratory syndrome. *Lancet* **395**, 1063–1077 (2020).
3. Cannalire, R. *et al.* SARS-CoV-2 Entry Inhibitors: Small Molecules and Peptides Targeting Virus or Host Cells. *Int. J. Mol. Sci.* **21**, 5707 (2020).
4. Jin, Z. *et al.* Structure of Mpro from COVID-19 virus and discovery of its inhibitors. *bioRxiv* 2020.02.26.964882 (2020) doi:10.1101/2020.02.26.964882.
5. Nadeem, M. S. *et al.* Origin, Potential Therapeutic Targets and Treatment for Coronavirus Disease (COVID-19). *Pathogens* **9**, 307 (2020).
6. Harrison, C. Drug researchers pursue new lines of attack against COVID-19. *Nat. Biotechnol.* **38**, 659–662 (2020).
7. Ghahremanpour, M. M. *et al.* Identification of 14 Known Drugs as Inhibitors of the Main Protease of SARS-CoV-2. *ACS Med. Chem. Lett.* **11**, 2526–2533 (2020).
8. Parnham, M. J. & Sies, H. The early research and development of ebselen. *Biochem. Pharmacol.* **86**, 1248–1253 (2013).

9. Santi, C., Scimmi, C. & Sancineto, L. Ebselen and Analogues: Pharmacological Properties and Synthetic Strategies for Their Preparation. *Molecules* **26**, 4230 (2021).

10. Jin, Z. *et al.* Structure of Mpro from SARS-CoV-2 and discovery of its inhibitors. *Nature* **582**, 289–293 (2020).

11. Weglarz-Tomczak, E. *et al.* Identification of ebselen and its analogues as potent covalent inhibitors of papain-like protease from SARS-CoV-2. *Sci. Rep.* **11**, 3640 (2021).

12. Zmudzinski, M. *et al.* Ebselen derivatives inhibit SARS-CoV-2 replication by inhibition of its essential proteins: PLpro and Mpro proteases, and nsp14 guanine N7-methyltransferase. *Sci. Rep.* **13**, 9161 (2023).

13. Menéndez, C. A., Byléhn, F., Perez-Lemus, G. R., Alvarado, W. & de Pablo, J. J. Molecular characterization of Ebselen binding activity to SARS-CoV-2 main protease. *Sci. Adv.* eabd3045 (2020) doi:10.1126/sciadv.abd0345.

14. Węglarz-Tomczak, E., Tomczak, J., Talma, M. & Brul, S. Ebselen as a highly active inhibitor of PL Pro CoV2. *bioRxiv* (2020) doi:10.1101/2020.05.17.100768.

15. Mukherjee, S. *et al.* Ebselen Inhibits Hepatitis C Virus NS3 Helicase Binding to Nucleic Acid and Prevents Viral Replication. *ACS Chem. Biol.* **9**, 2393–2403 (2014).

16. Chiou, J. *et al.* Ebselen as a potent covalent inhibitor of New Delhi metallo-β-lactamase (NDM-1). *Chem. Commun.* **51**, 9543–9546 (2015).

17. Favrot, L. *et al.* Mechanism of inhibition of Mycobacterium tuberculosis antigen 85 by ebselen. *Nat. Commun.* **4**, 2748 (2013).

18. Thenin-Houssier, S. *et al.* Ebselen, a Small-Molecule Capsid Inhibitor of HIV-1 Replication. *Antimicrob. Agents Chemother.* **60**, 2195–2208 (2016).

19. Leroux, F. *et al.* Identification of ebselen as a potent inhibitor of insulin degrading enzyme by a drug repurposing screening. *Eur. J. Med. Chem.* **179**, 557–566 (2019).

20. Lenardão, E. J., Santi, C. & Sancineto, L. *New Frontiers in Organoselenium Compounds*. (Springer International Publishing, 2018). doi:10.1007/978-3-319-92405-2.

21. Sies, H. & Parnham, M. J. Potential therapeutic use of ebselen for COVID-19 and other respiratory viral infections. *Free Radic. Biol. Med.* **156**, 107–112 (2020).

22. Amporndanai, K. *et al.* Inhibition mechanism of SARS-CoV-2 main protease by ebselen and its derivatives. *Nat. Commun.* **12**, 3061 (2021).

23. Sahoo, P. *et al.* Detailed Insights into the Inhibitory Mechanism of New Ebselen Derivatives against Main Protease (M pro) of Severe Acute Respiratory Syndrome Coronavirus-2 (SARS-CoV-2). *ACS Pharmacol. Transl. Sci.* (2022) doi:10.1021/acsptsci.2c00203.

24. Huff, S. *et al.* Discovery and Mechanism of SARS-CoV-2 Main Protease Inhibitors. *J. Med. Chem.* acs.jmedchem.1c00566 (2021) doi:10.1021/acs.jmedchem.1c00566.

25. Qiao, Z. *et al.* The Mpro structure-based modifications of ebselen derivatives for improved antiviral activity against SARS-CoV-2 virus. *Bioorg. Chem.* **117**, 105455 (2021).

26. Abian, O. *et al.* Structural stability of SARS-CoV-2 3CLpro and identification of quercetin as an inhibitor by experimental screening. *Int. J. Biol. Macromol.* **164**, 1693–1703 (2020).

27. Mangiavacchi, F. *et al.* Seleno-Functionalization of Quercetin Improves the Non-Covalent

Inhibition of Mpro and Its Antiviral Activity in Cells against SARS-CoV-2. *Int. J. Mol. Sci.* **22**, 7048 (2021).

28. Gomes, L. S. *et al.* Ecofriendly aminochalcogenation of alkenes: a green alternative to obtain compounds with potential anti-SARS-CoV-2 activity. *New J. Chem.* (2023) doi:10.1039/D2NJ06218F.

29. Krasowska, D. *et al.* Ultrasound-assisted synthesis of alkali metals diselenides (M2Se2) and their application for the gram-scale preparation of 2,2'-diselenobis(benzoic acid). *Arkivoc* **2019**, 24–37 (2019).

30. Begini, F. *et al.* Continuous flow synthesis of 2,2′-diselenobis(benzoic acid) and derivatives. *React. Chem. Eng.* **5**, 641–644 (2020).

31. Sancineto, L. *et al.* Design and Synthesis of DiselenoBisBenzamides (DISeBAs) as Nucleocapsid Protein 7 (NCp7) Inhibitors with anti-HIV Activity. *J. Med. Chem.* **58**, 9601–9614 (2015).

32. Nascimento, V. *et al.* Fast and easy conversion of ortho amidoaryldiselenides into the corresponding ebselen-like derivatives driven by theoretical investigations. *New J. Chem.* **44**, 9444–9451 (2020).

33. Pacuła, A. J. *et al.* New Chiral Ebselen Analogues with Antioxidant and Cytotoxic Potential. *Molecules* **22**, 492 (2017).

34. Obieziurska, M. *et al.* Bioselectivity Induced by Chirality of New Terpenyl Organoselenium Compounds. *Materials (Basel).* **12**, e3579 (2019).

35. Rizzuti, B. *et al.* Sub-Micromolar Inhibition of SARS-CoV-2 3CLpro by Natural Compounds. *Pharmaceuticals* **14**, 892 (2021).

36. Eberhardt, J., Santos-Martins, D., Tillack, A. F. & Forli, S. AutoDock Vina 1.2.0: New Docking Methods, Expanded Force Field, and Python Bindings. *J. Chem. Inf. Model.* **61**, 3891–3898 (2021).

37. Nogueira, C. W., Barbosa, N. V. & Rocha, J. B. T. Toxicology and pharmacology of synthetic organoselenium compounds: an update. *Arch. Toxicol.* **95**, 1179–1226 (2021).

38. Meister, A. Glutathione metabolism and its selective modification. *J. Biol. Chem.* **263**, 17205–8 (1988).

39. Silva, M. S. *et al.* Selenium-NMR Spectroscopy in Organic Synthesis: From Structural Characterization Toward New Investigations. *Asian J. Org. Chem.* **10**, 91–128 (2021).

40. Sands, K. N., Burman, A. L., Ansah-Asamoah, E. & Back, T. G. Chemistry Related to the Catalytic Cycle of the Antioxidant Ebselen. *Molecules* **28**, 3732 (2023).

41. Ma, C. *et al.* Ebselen, Disulfiram, Carmofur, PX-12, Tideglusib, and Shikonin Are Nonspecific Promiscuous SARS-CoV-2 Main Protease Inhibitors. *ACS Pharmacol. Transl. Sci.* **3**, 1265–1277 (2020).

42. Omage, F. B. *et al.* Diphenyl Diselenide and SARS-CoV-2: in silico Exploration of the Mechanisms of Inhibition of Main Protease (M pro) and Papain-like Protease (PL pro). *J. Chem. Inf. Model.* **63**, 2226–2239 (2023).

43. Rieder, G. S. *et al.* Computational analysis of the interactions between Ebselen and derivatives with the active site of the main protease from SARS-CoV-2. *Comput. Biol. Chem.* **107**, 107956

(2023).

44. Ma, C., Tan, H., Choza, J., Wang, Y. & Wang, J. Validation and invalidation of SARS-CoV-2 main protease inhibitors using the Flip-GFP and Protease-Glo luciferase assays. *Acta Pharm. Sin. B* **12**, 1636–1651 (2022).

45. Tan, H., Ma, C. & Wang, J. Invalidation of dieckol and 1,2,3,4,6-pentagalloylglucose (PGG) as SARS-CoV-2 main protease inhibitors and the discovery of PGG as a papain-like protease inhibitor. *Med. Chem. Res.* **31**, 1147–1153 (2022).

46. Heilmann, E. *et al.* A VSV-based assay quantifies coronavirus Mpro/3CLpro/Nsp5 main protease activity and chemical inhibition. *Commun. Biol.* **5**, 391 (2022).

47. Neese, F. The ORCA program system. *WIREs Comput. Mol. Sci.* **2**, 73–78 (2012).

48. Grimme, S., Ehrlich, S. & Goerigk, L. Effect of the damping function in dispersion corrected density functional theory. *J. Comput. Chem.* **32**, 1456–1465 (2011).

49. Grimme, S., Antony, J., Ehrlich, S. & Krieg, H. A consistent and accurate ab initio parametrization of density functional dispersion correction (DFT-D) for the 94 elements H-Pu. *J. Chem. Phys.* **132**, (2010).

50. Glendening, E. D. *et al.* NBO 7.0. (2018).

51. Rizzuti, B. *et al.* Rutin Is a Low Micromolar Inhibitor of SARS-CoV-2 Main Protease 3CLpro: Implications for Drug Design of Quercetin Analogs. *Biomedicines* **9**, 375 (2021).

52. Zhang, L. *et al.* Crystal structure of SARS-CoV-2 main protease provides a basis for design of improved α-ketoamide inhibitors. *Science (80-.).* **368**, 409–412 (2020).

53. Hanwell, M. D. *et al.* Avogadro: an advanced semantic chemical editor, visualization, and analysis platform. *J. Cheminform.* **4**, 17 (2012).

54. Santofimia-Castaño, P. *et al.* Intrinsically disordered chromatin protein NUPR1 binds to the C-terminal region of Polycomb RING1B. *Proc. Natl. Acad. Sci.* **114**, E6332–E6341 (2017).

55. Reed, L. J. & Muench, H. A simple method of estimating fifty percent endpoints. *Am. J. Epidemiol.* **27**, 493–497 (1938).